

Source-Free Domain Adaptation for SSVEP-based Brain-Computer Interfaces

Osman Berke Guney, Deniz Kucukahmetler and Huseyin Ozkan, *Member, IEEE*

Abstract—This paper presents a source free domain adaptation method for steady-state visually evoked potentials (SSVEP) based brain-computer interface (BCI) spellers. SSVEP-based BCI spellers assist individuals experiencing speech difficulties by enabling them to communicate at a fast rate. However, achieving a high information transfer rate (ITR) in most prominent methods requires an extensive calibration period before using the system, leading to discomfort for new users. We address this issue by proposing a novel method that adapts a powerful deep neural network (DNN) pre-trained on data from source domains (data from former users or participants of previous experiments) to the new user (target domain), based only on the unlabeled target data. This adaptation is achieved by minimizing our proposed custom loss function composed of self-adaptation and local-regularity terms. The self-adaptation term uses the pseudo-label strategy, while the novel local-regularity term exploits the data structure and forces the DNN to assign similar labels to adjacent instances. The proposed method prioritizes user comfort by removing the burden of calibration while maintaining an excellent character identification accuracy and ITR. In particular, our method achieves striking *201.15 bits/min* and *145.02 bits/min* ITRs on the benchmark and BETA datasets, respectively, and outperforms the state-of-the-art alternatives. Our code is available at <https://github.com/osmanberke/SFDA-SSVEP-BCI>

Index Terms—Steady-state visually evoked potentials, SSVEP, brain-computer interfaces, BCI, speller, deep learning, domain adaptation, domain generalization.

I. INTRODUCTION

Brain-computer interface (BCI) speller systems provide a means of communication for individuals who experience speech difficulties [1]. Owing to its non-invasive nature and practical usability, electroencephalography (EEG) is a typical choice for measuring the brain signals in those systems [2]. Steady-state visually evoked potential (SSVEP) is a brain response that is elicited by a visual object flickering with a certain frequency. Harmonics of the flickering frequency characterize the SSVEP response, and can be observed in the received signal when measured with EEG [3]. Because of this characteristic, SSVEP-based stimulation paradigms find substantial use in BCI speller systems [4] and are known to yield impressive speller performance in terms of character

identification (i.e. prediction) accuracy and information transfer rate (ITR) [5]. In these SSVEP-based BCI speller systems, the user chooses the character to be spelled from a collection of visuals flickering (each with a unique flickering frequency) on computer screen and attends fully by gazing. In the run time, the chosen character (the one intended to be spelled) can be identified by EEG signal classification. The goal is to maximize the ITR, enabling accurate character identification with relatively short stimulation [3]. Since EEG signal statistics vary significantly from one person to another, existing character identification algorithms of high ITRs (such as [3], [6]) require a quite tiring calibration process for each new user. This process has to be conducted before the actual system use begins, and includes new EEG experiments, collecting labeled data, pre-processing and algorithm training. As the typical user is a disabled individual, it is of immense importance to remove this burden of calibration for user comfort and allow an immediate plug-and-play system start.

To that end, transfer learning based methods [7], [8] aim domain generalization across participants¹ for knowledge extension to the new users. One example can be found in [7], which trains/develops algorithms using previously collected data of participants (source domains) and directly transfers to the new user (target domain) as is without requiring a calibration process. Although these methods provide user comfort, their character identification performances (i.e. prediction accuracy) are still far behind the best-performing methods (those requiring labeled data from target domain). On the other hand, one can consider source-free domain adaptation (SFDA) [9], [10] to achieve both user comfort and satisfactory identification performance. SFDA based approaches adapt the transferred method (originally trained with labeled data from source domains) to the target domain by using only unlabeled data from the target domain. Therefore, their (ones using unlabeled target data) performances are generally better than the domain generalization based ones (using no target data) of direct transfer. Since the SFDA approaches do not store, and actually discard, the data from source domains after training, they are called “source free”. Moreover, SFDA does not compromise the user comfort as it does not require a separate calibration or labeling process for the new user. Notice that the

O. B. Guney (corresponding author) is with the Department of Electrical and Computer Engineering at Boston University, Boston, MA, USA (e-mail: berke@bu.edu). D. Kucukahmetler is with the Department of Bioengineering, Imperial College London, London, UK (e-mail: d.kucukahmetler23@imperial.ac.uk). H. Ozkan is with the Faculty of Engineering and Natural Sciences at Sabanci University, Istanbul, Turkey (e-mail: huseyin.ozkan@sabanciuniv.edu). This work was supported in part by The Scientific and Technological Research Council of Turkiye (TUBITAK) under Contract 121E452. We thank P. Ciftcioglu and G. Coskun for their contributions in our experiments.

¹The term user refers to the actual end user of the system and the term participants refer to individuals participated in previously conducted EEG experiments or individuals who are old users when there is a new user joining. Moreover, similar to the machine learning literature, we refer to the participants as source domains and to the user as target domain.

SFDA framework is a suitable and natural choice for SSVEP-based BCI speller systems. As a new user interacts with the system, her/his unlabeled data continually accumulates and can be used for adapting the transferred method to gradually improve the initial transfer performance. Regarding the labeled data from source domains, it is typically available in large amounts and collected from offline past experiments with various healthy or disabled participants. One can even use the publicly available literature datasets for this purpose, such as benchmark [11] and BETA [12].

In this paper, in order to prioritize the user comfort while also achieving a decent performance, we propose a novel SFDA algorithm for the character identification in SSVEP-based BCI speller systems. Our algorithm adapts a previously trained (using source domains' labeled data) deep neural network (DNN) architecture (proposed in [3]) to the target domain (new user) based solely on the unlabeled data from the target domain. Additionally, in our method, there is no need to store the data of source domains and so we discard it after training the initial DNN. This helps us save memory and prevent any privacy concerns that can perhaps arise due to data being transferred from the past participants [9]. At the heart of our algorithm is a novel loss function that we introduce for the adaptation process, which consists of two terms: one is a self-adaptation loss \mathcal{L}_{sl} , and the other is a local-regularity loss \mathcal{L}_{ll} (along with standard L2 regularization). We compare our method with the strongest state-of-the-art alternatives [13], [14], [8] on two widely used publicly available datasets, benchmark [11] and BETA [12], and show that our method statistically significantly outperforms the others in terms of both accuracy and ITR.

II. RELATED WORK

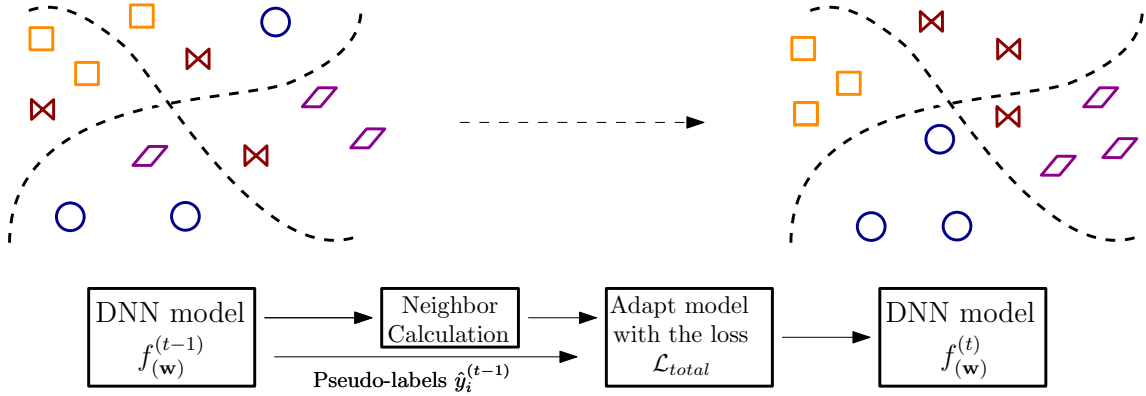
Character identification methods in the SSVEP-based BCI speller literature can be divided into two groups based on their calibration requirements on new users: user-dependent and user-independent. The user-dependent methods, such as [3], [6], [15], require a long and tiring calibration/preparation process (before the actual system use) for collecting labeled data from each new user, whereas the user-independent methods, such as [16], [17], do not. User-dependent methods generally exhibit superior performance, but that is at the cost of calibration discomfort [18] which -we consider- hinders the widespread use of SSVEP-based BCI speller systems. As we believe that the user comfort must not be compromised, we opt in this study for a method falling in the second group of user-independent methods. Our related work discussion here focuses on this second group, and we refer the interested readers to [18], [3] for detailed information about the first group of user-dependent.

The group of user-independent methods can be further divided into three categories, which are (i) completely training-free methods, (ii) domain generalization and (iii) domain adaptation based methods. Here, we use machine learning terms to stimulate novel perspectives for SSVEP character

identification by adopting from the literature of domain generalization and adaptation.

Completely training-free methods rely on mathematical models of the SSVEP signal characteristics. A frequently employed method in the literature [16] utilizes canonical correlation analysis (CCA) [19] to calculate the correlation coefficients between multi dimensional reference signals and the received multi-channel EEG signal. Those reference signals are formed for each character, consisting of sinusoids of the harmonics of corresponding flickering frequency. CCA identifies the combination of harmonics and channels that maximize the correlation coefficient between each reference signal (after harmonic combination) and the EEG signal (after channel combination) [16]. Then the character whose reference signal has the maximum correlation coefficient is declared as spelled. As in [3], we refer to this method as Standard-CCA throughout the paper. A filter-bank extension of Standard-CCA (FBCCA) is proposed in [17]. In FBCCA, multiple band-pass filters of different low cut-off frequencies first preprocess the input EEG, and Standard-CCA is then applied to each preprocessed signal. The intended character is predicted based on the weighted combination of calculated correlation coefficients. FBCCA has been demonstrated to achieve higher accuracy and ITR than Standard-CCA [17]. The advantage of these methods is that they are usable in a plug-and-play manner since they do not require any form of training. However, because of the same reason, they underperform, especially in the settings of short stimulation.

Domain generalization based methods leverage data from source domains to train/formulate models/templates that are directly applied in the target domain. For example, transfer template CCA (tt-CCA) [8] averages the data from source domains to form template signals for each character. Along with the correlation coefficient calculated as in the Standard-CCA method, tt-CCA calculates two additional correlation coefficients using the formed template signals and predicts the spelled character based on the combination of these three. The tt-CCA method's accuracy and ITR performances are superior to the Standard-CCA method [8]. Another domain generalization based method, combined-CCA (C3A) [14], predicts the spelled character in a way similar to tt-CCA, but the calculation of the correlation coefficients differs. In [7], the DNN architecture of [3] is first trained for each source domain. The resulting ensemble of DNNs is then transferred to the target domain, and the most k representative source domains' DNNs are used for spelled character prediction. It is reported that their ensemble of DNNs is the highest performing among such domain generalization based methods [7]. This category of methods is certainly practical as they do not require any labeled data from the target domain. However, since they do not make any sort of adaptation to the target domain, their performances are not as satisfying as the group of user-dependent or the category of domain adaptation (but generally better than the category of completely training-free). Also note that the domain adaptation based methods are usually built on top of the methods from this category, as explained next. Thus,



$$\mathcal{L}_{total}^{(t)}(\lambda) = \lambda \mathcal{L}_{sl}^{(t)} + (1 - \lambda) \mathcal{L}_{ll}^{(t)} + \beta ||\mathbf{w}||^2$$

Fig. 1: The outline of our source-free domain adaptation method and representative change in the DNN’s decision boundaries at two consecutive iterations during the adaptation are shown. Different shapes are for different classes. The adaptation starts with a DNN pre-trained using data from source domains, and it is carried out by minimizing the loss function \mathcal{L}_{total} that we also introduce, which consists of two main terms: self-adaptation \mathcal{L}_{sl} and local-regularity \mathcal{L}_{ll} . The self-adaptation component utilizes the pseudo-labeling approach, whereas the local-regularity component leverages the inherent structure of the data, forcing the adapted DNN to give similar labels to adjacent instances. Our method achieves *201.15 bits/min* and *145.02 bits/min* ITR results on the benchmark [11] and BETA [12] datasets, respectively. These results show that our proposed method provides significant ITR improvements over the state-of-the-art alternatives.

developing domain generalization based methods are equally important as developing domain adaptation based ones.

Domain adaptation based methods adapt to the target domain in an unsupervised fashion. One such method is online tt-CCA (ott-CCA), which extends tt-CCA by updating the transferred template signals using unlabeled target domain data. It is shown that ott-CCA improves the performance of tt-CCA [8]. Similarly, adaptive-C3A updates the transferred template signals in the C3A method, which also yields considerable performance enhancement [14]. A slightly different method, called online adaptive CCA (OACCA) [13], adapts FBCCA via new user-specific channel and harmonic combinations that are calculated based on techniques from [20] and [21]. We observe that to date, OACCA is the best-performing method in this category. Our preliminary simple pseudo-labeling adaptation, presented as a short conference proceeding (in Turkish) [22], also falls in this category. In that proceeding, we adapt the DNN architecture of [3] to the target domain by using only the self-adaptation term \mathcal{L}_{sl} . The present work, however, introduces several enhancements and novel features (such as the local regularity term \mathcal{L}_{ll}) as detailed in Section II-A. We compare our proposed method against the strongest alternatives OACCA [13], adaptive-C3A [14], and ott-CCA [8] methods. The experimental results show that our method delivers much higher identification accuracy and ITR figures, outperforming them altogether.

We also briefly highlight here a few related source-free domain adaptation methods from the machine/deep learning literature. A method referred to as SHOT, proposed in [23], adapts a network to the target domain. It freezes the

network’s last layer (the classifier part) and learns target-domain-specific features by adapting the remaining parts of the network (the feature extractor part) using pseudo-labeling. In [24], the authors propose a method called neighborhood reciprocity clustering (NRC) that exploits an intrinsic data structure and attempts to cluster similar instances. In another study [25], the authors approach the SFDA from the label noise perspective, where they use a regularizer to mitigate the label noise memorization problem. These studies inspired us in a very general sense. We used similar -but not the same- ideas in our adaptation method. For instance, our local-regularity loss term also exploits the structure of data, but our term is entirely different from the NRC method [25] and is designed to specifically utilize the characteristics of SSVEP signal. The SFDA literature is rapidly expanding; and we believe that in future studies, new ideas could be incorporated with our novel adaptation features here to generate more versatile machine/deep learning techniques.

A. Novel Contributions and Highlights

We propose in this paper a novel source-free unsupervised domain adaptation method that adapts the pre-trained DNN of [3] to the target domain particularly for practicality and user comfort in SSVEP-based BCI speller systems. The adaptation is carried out by minimizing our proposed custom loss function, composed of self-adaptation \mathcal{L}_{sl} and local-regularity \mathcal{L}_{ll} terms, based only on unlabeled data from target domain. We evaluate the performance of our method on two publicly available benchmark [11] and BETA [12] datasets. Our method demonstrates superior performance compared to the current state-of-the-art approaches, achieving an ITR of

201.15 bits/min on the benchmark dataset [11] and 145.02 bits/min on BETA. Our code is available for reproducibility at <https://github.com/osmanberke/SFDA-SSVEP-BCI>

- In our method, new users can immediately start using the system in a plug-and-play manner since there is no need for a calibration process to conduct tiring and long additional EEG experiments, pre-processing and algorithm training. In this sense, we particularly prioritize the user comfort. Also, the system performance continuously improves by adapting to the unlabeled data accumulated by the new user as s/he interacts with the system. Hence, we believe that our method has the potential to promote the widespread use of SSVEP-based BCI applications, such as gaming [26], in daily lives.
- To the best of our knowledge, this study presents (along with our preliminary short proceeding [22]) the first DNN based domain adaptation method in the SSVEP character identification literature. It also achieves the highest ITR in its own group of user-independent methods.
- A notable novelty in our work is the local regularity term \mathcal{L}_{ll} in the loss function that we introduce specifically for the SSVEP adaptation process. This term exploits the underlying data structure and forces the adapted DNN model f_w to give similar labels to neighbouring instances. It is worth noting that our regularity term here is technically completely different than that of the NRC method [24].
- Furthermore, regarding local regularity, we present a distinctive and innovative strategy for determining the set of neighbors dynamically (allowing a variable number of neighbors) for every SSVEP instance since (i) the user may spell some characters more often than others and (ii) the noise level/EEG signal statistics can change from one domain (person) to another or even temporally in the same domain (for the same person).
- Our method does also dynamically optimize the weights of the two loss terms, controlled by a λ parameter, for each target domain (new user) separately, since the degree of statistical similarity with the source domains (participants) can be quite different for each target domain.

III. PROBLEM DESCRIPTION

In the SSVEP-based EEG BCI speller systems, the spelled character is predicted out of M possibilities $y \in \{1, 2, \dots, M\}$. The prediction is based on the multi-channel EEG signal $\mathbf{x} \in \mathbb{R}^{C \times N_T}$ received during the stimulation², where C is the number of channels (EEG electrodes), $N_T = T \times F_s$ is the signal length, T (sec) is the stimulation duration and F_s is the sampling frequency (Hz). The goal is to maximize the information transfer rate (ITR) [27],

$$\text{ITR}(P, T) = (\log_2 M + P \log_2 P + (1 - P) \log_2 \left[\frac{1 - P}{M - 1} \right]) \frac{60}{T},$$

²We use the plain math type notation for scalar variables but the bold text type for vectors and matrices. For example, the multi-channel EEG signal is shown as \mathbf{x} instead of x .

which can be achieved by optimizing two incompatible objectives: maximizing the prediction accuracy P and minimizing the stimulation duration T [3]. Note that P and T are strongly coupled: When the data processing is optimal, the only way of improving accuracy (higher P) is to observe more data (longer T) which does not necessarily translate to a higher ITR. A viable strategy here is to maximize the prediction accuracy for a fixed T , yielding $P^*(T)$, and choose $T^* = \arg \max_T \text{ITR}(P^*(T), T)$ as the optimal stimulation duration [3]. For a given fixed stimulation duration T , the task of maximizing the prediction accuracy P can be studied as a multi-class classification problem, i.e., character identification.

IV. METHOD

We constrain the above-described multi-class classification problem with user comfort as explained in Section I. Particularly, our aim is to remove the burden of calibration process from the user and allow an immediate plug-and-play system start. Therefore, unsupervised and source-free domain adaptation is a viable approach, where unlabeled data from target domain is exploited.

Before we explain the details, let us assume that a set of labeled EEG data instances from a collection of participants (source domains) is available: $\{(\mathbf{x}_i^l, y_i^l)\}_{i=1}^{D_l}\}_{l=1}^{N_{tr}}$, where N_{tr} is the number of source domains, and D_l is the total number of EEG instances from l 'th participant. We also use $\mathbf{z}_i^l \in \{0, 1\}^{M \times 1}$ as one-hot encoding of label y_i^l such that $\mathbf{z}_{i, y_i^l}^l = 1$, where $\mathbf{z}_{i, y_i^l}^l$ is the y_i^l 'th element of \mathbf{z}_i^l , and 0 otherwise. Additionally, a set of unlabeled EEG data instances from the new user (target domain) is denoted by $\{\mathbf{x}_i\}_{i=1}^N$.

We start by transferring a powerful deep neural network f_w that is pre-trained with data $\{(\mathbf{x}_i^l, y_i^l)\}_{i=1}^{D_l}\}_{l=1}^{N_{tr}}$ from source domains (cf. [3] for details of the architecture) to the target domain, yielding a high enough initial accuracy. Then, we adapt the network f_w (w keeps the network parameters) to the target domain with unlabeled data generated in the process as the user (target domain) interacts with the system. Thus, the initial transfer accuracy improves with the introduced unsupervised adaptation. The network f_w gives a soft response $f_w(\mathbf{x}_i) = \mathbf{s}_i \in [0, 1]^{M \times 1}$ to the input \mathbf{x}_i with the prediction \hat{y}_i being the index of the maximum in \mathbf{s}_i , i.e., $\hat{y}_i = \arg \max_j \mathbf{s}_{i,j}$.

Our method is mainly based on a novel loss function that we introduce for the unsupervised adaptation of the transferred network f_w . This introduced loss, which is minimized using unlabeled data from the target domain with expectation-maximization (EM) type of iterations [28], consists of two terms: self-adaptation \mathcal{L}_{sl} and local-regularity \mathcal{L}_{ll} terms.

Self-Adaptation Loss \mathcal{L}_{sl} : In the presence of true target data labels y_i , the model f_w would be adapted to target domain by minimizing the standard cross entropy loss:

$$-\frac{1}{N} \sum_{i=1}^N \sum_{j=1}^M \mathbf{z}_{i,j} \log(\mathbf{s}_{i,j}) = -\frac{1}{N} \sum_{i=1}^N \log(\mathbf{s}_{i, y_i}),$$

where the equality follows because the y_i 'th index of the one-hot encoding vector \mathbf{z}_i equals to 1, and the other indexes are 0 (with $0 \log 0 = 0$).

However, since we do not have the true labels in the SFDA setting, predictions \hat{y}_i of the model can be used as pseudo-labels for adaptation (hence the model $f_{\mathbf{w}}$ is updated) which in turn yields new predictions and a new adaptation. This defines a single iteration which we repeat until convergence. Let $\mathbf{w}^{(t)}$ be the adapted parameters and let $\mathbf{s}_i^{(t)}$ and $y_i^{(t)}$ be the network soft responses and predictions, respectively, for the input \mathbf{x}_i at the end of iteration t , i.e., $\mathbf{s}_i^{(t)} = f_{\mathbf{w}^{(t)}}(\mathbf{x}_i)$ and $\hat{y}_i^{(t)} = \arg \max_j \mathbf{s}_{i,j}^{(t)}$. Within this scheme, such EM type of iterations define our first term of self-adaptation loss as

$$\mathcal{L}_{sl}^{(t)} = -\frac{1}{N} \sum_{i=1}^N \log(\mathbf{s}_{i, \hat{y}_i^{(t)}}^{(t)}). \quad (1)$$

The efficacy of minimizing loss functions using pseudo-labels has been previously shown in many unsupervised [29] and semi-supervised [30], [31], [32] settings. In effect, the network learns classes that are well separated in low-density regions by minimizing the class overlaps [30]. It is also equivalent to entropy regularization [31], which aims to benefit from unlabeled data in the maximum a posteriori sense. Another perspective can be taken from the concept of dropout regularization, proposed in [33] to reduce overfitting. When the dropout layer is used in any model, in the phase of training, a different part (thinned version) of the network is used every time it forms a response. Whereas in the phase of testing, responses are always formed based on the full network (no node dropping). Responses of full network are generally better (having less errors) than those of a partial network, cf. Fig. 11 in [33]. Now, notice that the network [3] that we transfer (after training with source domains' data) to the target domain does also include dropout layers. Namely, the full network $f_{\mathbf{w}^{(t)}}$ is used when generating the pseudo-labels and partial networks derived from $f_{\mathbf{w}^{(t)}}$ with node dropping are used when minimizing the self adaptation loss in (1). Hence, the quality difference between the responses of the model obtained during training and testing can explain performance gains in using pseudo-labels, as also observed in our short proceeding (presenting the preliminary results of the present work in Turkish) [22].

Although minimizing self-adaptation loss is effective, it does not take into account the structure of the available unlabeled data from target domain. We next explain our proposed local-regularity loss \mathcal{L}_{ll} that exploits the data structure.

Local-Regularity Loss \mathcal{L}_{ll} : The idea behind local regularity is that close (or similar) enough data instances should attain similar labels (Fig. 1), which has been successfully exploited in many past studies of algorithm design. A couple of examples can be found in source-free domain adaptation [23], [24], metric learning [34], [35], and kernel learning [36]. Accordingly, we use the correlation coefficient³ as a measure

³Since the SSVEP instances we consider here are multidimensional (\mathbf{x}_i 's are in the matrix form of dimension $C \times N_T$), we calculate the correlation coefficient $\rho(\mathbf{x}_i, \mathbf{x}_j)$ after applying a common channel combination \mathbf{w}_c to both instances. The details of selecting the channel combination and calculations are explained in Appendix.

Algorithm 1 Source-Free Adaptation of DNN $f_{\mathbf{w}}$

- 1: **Input:** Unlabeled data instances $\{\{\mathbf{x}_i\}\}_{i=1}^N$ from the user (target domain) and pre-trained model's weights $\mathbf{w}^{(0)}$.
 - 2: **Parameters:** Learning rate $\alpha = 0.0001$, L2 regularization weight $\beta = 0.001$, maximum number of trials $B = 3$ and epochs $J = 50$, and the set of candidate $\lambda \in \Delta = \{0, 0.2, \dots, 1\}$.
 - 3: Let the previous iteration $t - 1$ be denoted by $t' = t - 1$.
 - 4: **for** $\lambda \in \Delta$ **do**
 - 5: Calculate the initial clustering score $m^{(0)}(\lambda)$.
 - 6: Set iteration $t = 1$ and trial $b = 0$.
 - 7: **repeat**
 - 8: **for** $j = 0$ **to** $J - 1$ **do**
 - 9: Apply gradient descent to update:
 $\mathbf{w}^{(t'+j+1)} = \mathbf{w}^{(t'+j)} - \alpha \times \nabla_{\mathbf{w}^{(t'+j)}} \mathcal{L}_{total}^{(t'+j)}(\lambda)$.
 - 10: **end for**
 - 11: Calculate the clustering score $m^{(t)}(\lambda)$.
 - 12: **if** $m^{(t)}(\lambda) > m^{(t')}(\lambda)$ **then**
 - 13: Calculate the new predictions $\hat{y}_i^{(t)}$ for all i .
 - 14: $t \leftarrow t + 1$.
 - 15: Set trial $b = 0$.
 - 16: **else**
 - 17: $b \leftarrow b + 1$
 - 18: **end if**
 - 19: **until** $b = B$ (terminal).
 - 20: **end for**
 - 21: $\lambda_{\max} = \arg \max_{\lambda \in \Delta} m^{(t)}(\lambda)$
 - 22: **Return:** $\mathbf{w}^{(t)}(\lambda_{\max})$
 - 23: **Comment:** Our code is available for reproducibility at <https://github.com/osmanberke/SFDA-SSVEP-BCI>
-

to define closeness (similarity) and obtain our local-regularity loss \mathcal{L}_{ll} as

$$\mathcal{L}_{ll}^{(t)} = -\frac{1}{N} \sum_{i=1}^N \frac{1}{k_i} \sum_{j=1}^{k_i} \log(\mathbf{s}_{i, \hat{y}_{I_i(j)}}^{(t)}), \quad (2)$$

where

- I_i is the set of indexes that are sorted in descending order based on the correlation coefficient values between the target domain instances $\{\mathbf{x}_j\}_{j=1, j \neq i}^N$ and the target domain instance \mathbf{x}_i . Namely, $\mathbf{x}_{I_i(1)}$ is the most correlative (closest) to \mathbf{x}_i .
- k_i is the number of neighbors considered for the instance \mathbf{x}_i . Note that the neighborhood size is not fixed, and allowed to vary across instances. This is because the user might well spell certain characters more often than others, or the neighborhood size (set of similar instances) can shrink or expand depending on the noise level which can vary from domain to domain or even from instance to instance in the same domain.
- Superscript $^{(t)}$ denotes the iterations as described earlier.

The minimization of this loss enforces the transferred network $f_{\mathbf{w}^{(t)}}$ to give similar predictions to instances that are in

close proximity. Note that the correlation coefficient value is inversely proportional to the squared Euclidean distance after centering and unit-norm normalization. In fact, most of the methods explained in Section II such as [7], [13], [17] use the correlation coefficient as a suitable metric for measuring similarities between SSVEP signals.

As for determining the variable neighborhood size k_i properly, it is reasonable to assume that the correlation coefficients between the instance \mathbf{x}_i and its neighboring instances that should share similar labels with \mathbf{x}_i are much higher compared to the other instances. As a result, one could expect a significant drop from the k_i 'th highest correlation coefficient to the next $k_i + 1$ 'th highest:

$$\frac{\rho(\mathbf{x}_i, \mathbf{x}_{I_i(k_i)}) - \rho(\mathbf{x}_i, \mathbf{x}_{I_i(k_i+1)})}{|\rho(\mathbf{x}_i, \mathbf{x}_{I_i(k_i)})|} \geq \delta,$$

where the left hand side of the inequality describes the drop in percentage and the right hand side δ is a predetermined threshold testing the significance of the drop. The neighborhood size k_i is taken from the point of significant drop.

Total Loss: Combination of the self-adaptation (1) and local regularity (2) terms, along with an L2 regularization, yield the total loss

$$\mathcal{L}_{total}^{(t)}(\lambda) = \lambda \mathcal{L}_{sl}^{(t)} + (1 - \lambda) \mathcal{L}_{ll}^{(t)} + \beta \|\mathbf{w}\|^2, \quad (3)$$

where $\lambda \in [0, 1]$ controls the contribution of individual loss terms and β is the weight of L2 regularization. We experimentally set $\beta = 0.001$.

Furthermore, a dynamic parameter selection procedure is proposed for λ as follows. Firstly, we adapt the DNN $f_{\mathbf{w}^{(t-1)}}$ to the target domain by minimizing $\mathcal{L}_{total}^{(t-1)}(\lambda)$ separately for every value from a set of candidates $\lambda \in \Lambda$, yielding $\mathbf{w}^{(t)}(\lambda)$ for the adapted parameters and $\hat{y}_i^{(t)}(\lambda)$ for the predictions. Then, to decide which of the adapted network parameters $\{\mathbf{w}^{(t)}(\lambda) : \lambda \in \Lambda\}$ is to be used for a final prediction (either at the end of iterations or intermediately if needed), we check how well each adapted parameters $\mathbf{w}^{(t)}(\lambda)$ cluster the unlabeled target domain data. The silhouette clustering metric [37] is used for that purpose, which generates a score $m_i^{(t)}(\lambda)$ to assess how well an instance \mathbf{x}_i is clustered based on the difference between the tightness $a_i^{(t)}(\lambda)$ of \mathbf{x}_i to its own cluster and separation $b_i^{(t)}(\lambda)$ of \mathbf{x}_i from other clusters:

$$\begin{aligned} a_i^{(t)}(\lambda) &= \frac{1}{q_{\hat{y}_i^{(t)}(\lambda)}^{(t)} - 1} \sum_{\substack{j=1 \\ j \neq i}}^N d(\mathbf{x}_j, \mathbf{x}_i) \mathbb{I}(\hat{y}_j^{(t)}(\lambda) = \hat{y}_i^{(t)}(\lambda)), \\ b_i^{(t)}(\lambda) &= \min_{\substack{k \in \{1, \dots, M\} \\ \setminus \{\hat{y}_i^{(t)}(\lambda)\}}} \frac{1}{q_k^{(t)}(\lambda)} \sum_{\substack{j=1 \\ j \neq i}}^N d(\mathbf{x}_j, \mathbf{x}_i) \mathbb{I}(\hat{y}_j^{(t)}(\lambda) = k), \\ m_i^{(t)}(\lambda) &= \frac{b_i^{(t)}(\lambda) - a_i^{(t)}(\lambda)}{\max(a_i^{(t)}(\lambda), b_i^{(t)}(\lambda))}, \end{aligned} \quad (4)$$

where

- $\mathbb{I}(\cdot)$ is the indicator function that returns 1 if its condition is satisfied (otherwise 0), $q_k^{(t)}(\lambda)$ is the total number

of instances labeled as k by the DNN with parameters $\mathbf{w}^{(t)}(\lambda)$, i.e., $q_k^{(t)}(\lambda) = \sum_{j=1}^N \mathbb{I}(\hat{y}_j^{(t)}(\lambda) = k)$,

- $d(\mathbf{x}_i, \mathbf{x}_j)$ is a distance metric derived from the correlation coefficient as $d(\mathbf{x}_j, \mathbf{x}_i) = 1 - \rho(\mathbf{x}_j, \mathbf{x}_i)$, which is equivalent to cosine distance if \mathbf{x}_i 's are zero mean signals,
- $a_i^{(t)}(\lambda)$ is the average distance from \mathbf{x}_i to the other instances of the same predicted label, i.e., $a_i^{(t)}(\lambda)$ equals to 1 if $q_{\hat{y}_i^{(t)}(\lambda)}^{(t)} = 1$,
- $b_i^{(t)}(\lambda)$ is the minimum average distance from \mathbf{x}_i to the instances of another cluster (of a different predicted label) with the minimization being over all other clusters,
- superscript (t) denotes the iterations as described earlier.

The overall silhouette clustering score for the predictions of the model with parameters $\mathbf{w}^{(t)}(\lambda)$ is the average of the silhouette scores of all the instances, i.e., $m^{(t)}(\lambda) = \sum_{i=1}^N m_i^{(t)}(\lambda) / N$. The network parameters $\mathbf{w}^{(t)}(\lambda)$ with the highest silhouette clustering score $m^{(t)}(\lambda)$ is selected.

The adaptation is continued separately for each λ until convergence that is controlled with the overall silhouette clustering score $m^{(t)}(\lambda)$. It is terminated, if the minimization of $\mathcal{L}_{total}^{(t)}(\lambda)$ does not yield a sufficient improvement in the clustering score compared to the previous iteration $m^{(t-1)}(\lambda)$ over B consecutive trials. At each trial of an iteration t , the adaptation is started with the DNN's weights $\mathbf{w}^{(t-1)}$ of the previous iteration $t - 1$. The reason for using these multiple trials is that the weights converge to a different state at each trial because of the randomness caused by the dropout layers. Also note that J epochs are employed for stable training at each iteration. The outline of our adaptation algorithm is given in Algorithm 1.

Lastly, prediction confidences have been shown to be useful in the unsupervised learning literature [29], [38]. We also take into account the confidence aspect in our method, because each instance is clustered with varying degrees of confidence; while some instances are clustered well, others are not. Therefore, we use the pseudo-labels of only those instances which are clustered well with positive silhouette values m_i^λ . The reason behind this approach is that an instance having a negative silhouette score implies that there exists a cluster closer to this instance than the cluster it is attributed to. Hence, instances having negative silhouette scores are more likely to be misclassified. To avoid updating the DNN using the pseudo-labels that are likely to be incorrect, we update with only the pseudo-labels of the instances having a positive silhouette score. The details of our confidence study as well as all the other implementation details are given in Appendix.

V. PERFORMANCE EVALUATIONS

We compare our source-free domain adaptation method (Algorithm 1) with three state-of-the-art domain adaptation alternatives from the literature, OACCA [13], adaptive-C3A [14] and ott-CCA [8]. The presented comparisons are based on the large scale (EEG experiments with 105 participants in total) benchmark [11] and the BETA [12] datasets which are

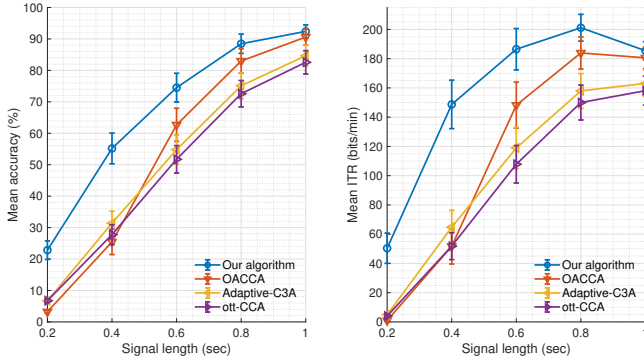


Fig. 2: The mean classification accuracy on the left and the mean information transfer rate (ITR) on the right are presented across all 35 users in the benchmark dataset [11], together with the standard errors indicated by the bars.

publicly available and widely used in the literature. The performance evaluation is conducted in a leave-one-participant-out fashion. One participant is reserved and considered as the user (target domain), while the remaining participants' data (source domains) are exploited to obtain the pre-trained DNN f_w of [3]. We next adapt the DNN to the target domain in an unsupervised manner, using all the unlabeled data of the target domain, and calculate the accuracy and ITR performance with true labels at the end of the adaptation. This procedure is repeated for each participant, so we have 35 and 70 repetitions for the benchmark and BETA datasets, respectively.

The adaptation is continued until the silhouette clustering metric converges in our method (Algorithm 1). On the contrary, there is no convergence control in the compared methods since their solutions do not involve losses or convergences. To ensure a fair comparison, nonetheless, we apply the same procedure to the compared methods as well. Namely, the adaptation is continued until all the predictions remain the same for two successive iterations in the compared methods. The same input is given to all compared methods to receive their initial predictions, which are then used as pseudo-labels for updating their template/channel and harmonic combinations as explained in their respective papers. This resumes iteratively until the pseudo-labels are no longer updated in the new iteration, leading to a unique number of iterations for each method. Similarly, the performance is evaluated with true labels of the participant reserved as the target domain.

A. Datasets

We use two large scale datasets for the purpose of performance evaluations: the benchmark [11] and BETA [12] which include SSVEP signals of 35 and 70 healthy participants recorded with EEG from 64 channels whilst performing the BCI spelling task. In terms of the experimental setups of the task, a visual representation of 5×8 character matrix in the benchmark and a keyboard layout in BETA consisting of alphanumeric characters and symbols (e.g. blank space) are presented to the participant. In each dataset, there are a

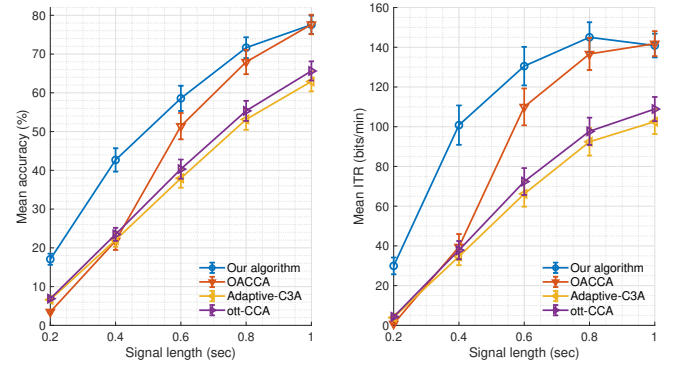


Fig. 3: The mean classification accuracy on the left and the mean information transfer rate (ITR) on the right are presented across all 70 users in the BETA dataset [12], together with the standard errors indicated by the bars.

total of 40 characters, each character has a unique flickering frequency in the range from 8 to 15.8 Hz with 0.2 Hz increment, and there is at least 0.5π phase difference between adjacent characters. The participants are instructed to gaze toward a 0.5 seconds visual cue (i.e. a red square) around the character to be spelled followed by a flickering period and an offset (i.e. resting phase). Consequently, 6-second SSVEP signals are recorded for each 40 character in 6 blocks in the benchmark, and 4-second (3-second) SSVEP signals for the first 15 participants (for the remaining 55 participants) are recorded for each 40 character in 4 blocks in BETA (including 0.5 seconds of gaze shift and 0.5 seconds for offset). Importantly, the SSVEP signals for the benchmark dataset were collected in a shielded lab environment whereas BETA signals were collected outside the lab. Hence, BETA signals are of poorer quality, presenting a more challenging character recognition problem. More detailed information about the experimental setup and data collection can be found in [11] for the benchmark dataset and in [12] for BETA.

B. Results and Discussion

The mean (across users) classification accuracy and mean ITR with the standard errors are reported for the signal duration T in the range $T \in \{0.2, 0.4, \dots, 1.0\}$. Also, 0.5 seconds of gaze shift time that exists in both datasets is taken into account when calculating ITR. In all of the methods, a pre-determined set of 9 channels (Pz, PO3, PO5, PO4, PO6, POz, O1, Oz, and O2) are used from the occipital and parietal regions.

The results presented in Fig. 2 and Fig. 3 show that our method significantly outperforms the other methods by achieving 201.15 bits/min and 145.02 bits/min maximum ITRs on the benchmark and BETA datasets, respectively. The closest performance to that of our method is obtained by the OACCA method which achieves 183.92 bits/min on the benchmark and 141.80 bits/min on BETA. Our method's superiority is more pronounced when the signal (stimulation) duration is shorter (i.e. 0.2, 0.4, 0.6 seconds). For instance, with $T = 0.4$

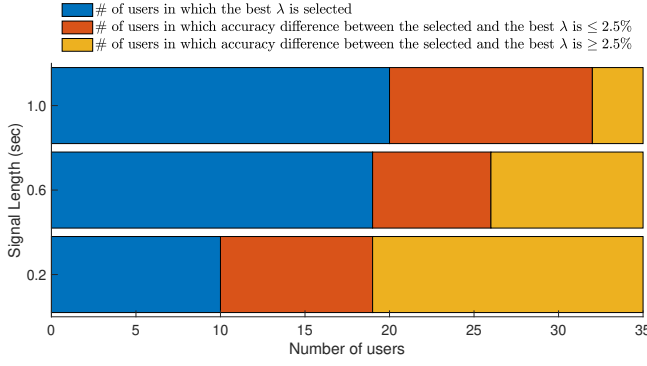


Fig. 4: Our λ selection is illustrated with the benchmark dataset [11] for three different signal lengths, 0.2, 0.6 and 1 seconds. The graph represents the distribution of users into three specific performance intervals of accuracy comparisons between the selected λ and the best λ .

seconds, we achieve 148.72 bits/min (benchmark) and 100.81 bits/min ITR (BETA) whereas the closest performance among compared methods is 64.72 bits/min (Adaptive-C3A) for the benchmark dataset and 39.50 bits/min (OACCA) for BETA. Thus, these results suggest that we significantly improve the literature for short signal lengths in the unsupervised setting, while clearly maintaining the lead across all signal lengths. To our best knowledge, these performance figures are the best achieved results in our method’s category of user independent methods (those which do not require calibration) in the literature (cf. Section II).

Fig. 4 and Fig. 5 analyze our λ selection. Recall that in our method (Algorithm 1), the pre-trained DNN is adapted to the target domain multiple times, each time with a different λ chosen from $\Lambda = \{0, 0.2, 0.4, 0.6, 0.8, 1\}$. In hindsight, the best λ (which is unknown in the process) is the one yielding the highest accuracy when tested with true labels at the end of the adaptation. In this analysis, we check the deviation between the accuracy performance of the best λ and that of λ selected according to the overall silhouette score as explained in Section IV. Three performance intervals of accuracy comparisons are considered: (i) no deviation (the best λ is selected successfully), (ii) deviation within a margin of 2.5% (the best λ is selected approximately), and (iii) out of margin deviation (the best λ is missed). The reason for using $1/40 = 2.5\%$ as the margin threshold is that it is the chance level in the current classification problem.

In the benchmark dataset (35 users in total), the best λ is successfully selected for 10, 19 and 20 users in the cases of 0.2, 0.6 and 1 seconds of stimulation, respectively. In the BETA dataset (70 users in total), the best λ is successfully selected for 8, 26 and 36 users in the cases of 0.2, 0.6 and 1 seconds of stimulation, respectively. Therefore, our λ selection improves significantly with the increasing signal length T (stimulation duration), because the signal-to-noise ratio (SNR) of the SSVEP harmonics increases with longer stimulation leading to more reliable silhouette clustering metric computa-

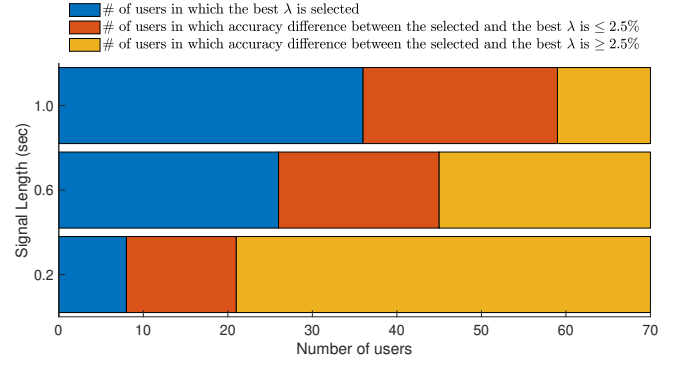


Fig. 5: Our λ selection is illustrated with the BETA dataset [12] for three different signal lengths, 0.2, 0.6 and 1 seconds. The graph represents the distribution of users into three specific performance intervals of accuracy comparisons between the selected λ and the best λ .

tions. The SNR level also explains having better λ selection for the benchmark dataset compared to BETA as the BETA signals collected outside lab are of lower SNR and noisier.

C. Statistical Significance Analyses

For each $T \in \{0.2, 0.4, 0.6, 0.8, 1\}$, we conduct 3 paired t-tests, pairing our proposed adaptation method (Algorithm 1) with the compared methods in Fig. 2 and Fig. 3. Unadjusted p-values are reported, and we call the observed difference as “statistically significant” (*) if the p-value is less than $\frac{0.05}{3}$ and “statistically highly significant” (**) if the p-value is less than $\frac{0.05}{3 \times 5}$. For the statistically significant case, single Bonferroni correction is applied by dividing 0.05 by 3, since for each T there are 3 comparisons. And for the statistically highly significant case, we apply double Bonferroni correction by 15, since across all methods and T choices there are $3 \times 5 = 15$ comparisons.

In the case of the benchmark dataset: In terms of the accuracy (Fig. 2), the least significant difference between our method (Algorithm 1) and the compared methods is observed with (i) ott-CCA (** $p = 3.49 \times 10^{-7}$) for $T = 0.2$, (ii) OACCA (** $p = 2.26 \times 10^{-7}$) for $T = 0.4$, (iii) OACCA (* $p = 0.94 \times 10^{-2}$) for $T = 0.6$, (iv) OACCA (* $p = 0.01$) for $T = 0.8$, (v) OACCA ($p = 0.07$) for $T = 1.0$. For $T = 1.0$, the difference with OACCA is not significant; but highly significant (**) with all the others. In terms of the ITR (Fig. 2), the least significant difference between our method (Algorithm 1) and the compared methods is observed with (i) ott-CCA (** $p = 3.40 \times 10^{-5}$) for $T = 0.2$, (ii) OACCA (** $p = 6.06 \times 10^{-8}$) for $T = 0.4$, (iii) OACCA (** $p = 0.32 \times 10^{-2}$) for $T = 0.6$, (iv) OACCA (* $p = 0.44 \times 10^{-2}$) for $T = 0.8$, and (v) OACCA ($p = 0.09$) for $T = 1$. For $T = 1.0$, the difference with OACCA is not significant; but highly significant (**) with all the others.

In the case of the BETA dataset: In terms of the accuracy (Fig. 3), the least significant difference between our method (Algorithm 1) and the compared methods is observed with (i) ott-CCA (** $p = 2.77 \times 10^{-12}$) for $T = 0.2$, (ii) OACCA

($**p = 1.32 \times 10^{-11}$) for $T = 0.4$, (iii) OACCA ($*p = 0.51 \times 10^{-2}$) for $T = 0.6$, (iv) OACCA ($p = 0.02$) for $T = 0.8$, (v) OACCA ($p = 0.96$) for $T = 1.0$. For $T = 0.8$ and $T = 1.0$, the difference with OACCA is not significant; but highly significant ($**$) with all the others. In terms of the ITR (Fig. 3), the least significant difference between our method (Algorithm 1) and the compared methods is observed with (i) Adaptive-C3A ($**p = 3.60 \times 10^{-9}$) for $T = 0.2$, (ii) OACCA ($**p = 5.38 \times 10^{-10}$) for $T = 0.4$, (iii) OACCA ($**p = 0.33 \times 10^{-2}$) for $T = 0.6$, (iv) OACCA ($p = 0.02$) for $T = 0.8$, and (v) OACCA ($p = 0.76$) for $T = 1.0$. For $T = 0.8$ and $T = 1.0$, the difference with OACCA is not significant; but highly significant ($**$) with all the others.

VI. CONCLUSION

In this study, we proposed a source free domain adaptation method for steady-state visually evoked potential (SSVEP) based brain-computer interfaces (BCIs). Our method adapts a deep neural network (DNN) architecture (pre-trained with labeled data from source domains) to a new user (target domain) using only unlabeled target data by minimizing our proposed novel loss function. There are two main terms in the proposed loss function: self-adaptation and local-regularity. The self-adaptation term utilizes the pseudo-label strategy. The local-regularity term takes advantage of the data structure and forces the DNN to give similar labels to neighbored instances. We experimented with commonly used and publicly available two large scale datasets, which are the benchmark and BETA datasets. Our method is observed to outperform all the compared alternatives in terms of accuracy and information transfer rate, achieving to the best of our knowledge the best performance within its own category of calibration-free methods. In our design, we specifically prioritized the user comfort by not requiring any calibration or preparation process and allowed an immediate system start. Hence, our method can be directly used in plug-and-play manner. In this sense, we believe that the presented work strongly promotes the spread of SSVEP-based BCI systems in daily life.

REFERENCES

- [1] H. Nezamfar, S. S. Mohseni Salehi, M. Moghadamfalahi, and D. Erdogmus, "Flashtypetm: A context-aware c-vep-based bci typing interface using eeg signals," *IEEE Journal of Selected Topics in Signal Processing*, vol. 10, no. 5, pp. 932–941, 2016.
- [2] B. Kadioglu, I. Yildiz, P. Closas, and D. Erdogmus, "M-estimation-based subspace learning for brain computer interfaces," *IEEE Journal of Selected Topics in Signal Processing*, vol. 12, no. 6, pp. 1276–1285, 2018.
- [3] O. B. Guney, M. Oblokulov, and H. Ozkan, "A deep neural network for ssvep-based brain-computer interfaces," *IEEE Transactions on Biomedical Engineering*, vol. 69, no. 2, pp. 932–944, 2022.
- [4] M. Li, D. He, C. Li, and S. Qi, "Brain-computer interface speller based on steady-state visual evoked potential: A review focusing on the stimulus paradigm and performance," *Brain Sciences*, vol. 11, no. 4, 2021.
- [5] E. Yin, Z. Zhou, J. Jiang, Y. Yu, and D. Hu, "A dynamically optimized ssvep brain-computer interface (bci) speller," *IEEE Transactions on Biomedical Engineering*, vol. 62, no. 6, pp. 1447–1456, 2015.
- [6] Y. Li *et al.*, "Convolutional correlation analysis for enhancing the performance of ssvep-based brain-computer interface," *IEEE Transactions on Neural Systems and Rehabilitation Engineering*, vol. 28, no. 12, pp. 2681–2690, 2020.
- [7] O. B. Guney and H. Ozkan, "Transfer learning of an ensemble of dnns for ssvep bci spellers without user-specific training," *Journal of Neural Engineering*, vol. 20, p. 016013, jan 2023.
- [8] P. Yuan, X. Chen, Y. Wang, X. Gao, and S. Gao, "Enhancing performances of SSVEP-based brain-computer interfaces via exploiting inter-subject information," *Journal of Neural Engineering*, vol. 12, p. 046006, jun 2015.
- [9] K. Xia, L. Deng, W. Duch, and D. Wu, "Privacy-preserving domain adaptation for motor imagery-based brain-computer interfaces," *IEEE Transactions on Biomedical Engineering*, vol. 69, no. 11, pp. 3365–3376, 2022.
- [10] P. Lee, S. Jeon, S. Hwang, M. Shin, and H. Byun, "Source-free subject adaptation for eeg-based visual recognition," in *2023 11th International Winter Conference on Brain-Computer Interface (BCI)*, pp. 1–6, Feb 2023.
- [11] Y. Wang, X. Chen, X. Gao, and S. Gao, "A benchmark dataset for ssvep-based brain-computer interfaces," *IEEE Transactions on Neural Systems and Rehabilitation Engineering*, vol. 25, no. 10, pp. 1746–1752, 2017.
- [12] B. Liu, X. Huang, Y. Wang, X. Chen, and X. Gao, "Beta: A large benchmark database toward ssvep-bci application," *Frontiers in Neuroscience*, vol. 14, p. 627, 2020.
- [13] C. M. Wong, Z. Wang, M. Nakanishi, B. Wang, A. Rosa, P. Chen, T.-P. Jung, and F. Wan, "Online adaptation boosts ssvep-based bci performance," *IEEE Transactions on Biomedical Engineering*, pp. 1–1, 2021.
- [14] N. R. Waytowich, J. Faller, J. O. Garcia, J. M. Vettel, and P. Sajda, "Unsupervised adaptive transfer learning for steady-state visual evoked potential brain-computer interfaces," in *IEEE International Conference on Systems, Man, and Cybernetics (SMC)*, pp. 004135–004140, 2016.
- [15] M. Nakanishi, Y. Wang, X. Chen, Y. Wang, X. Gao, and T. Jung, "Enhancing detection of ssveps for a high-speed brain speller using task-related component analysis," *IEEE Transactions on Biomedical Engineering*, vol. 65, no. 1, pp. 104–112, 2018.
- [16] Z. Lin, C. Zhang, W. Wu, and X. Gao, "Frequency recognition based on canonical correlation analysis for ssvep-based bcis," *IEEE Transactions on Biomedical Engineering*, vol. 53, no. 12, pp. 2610–2614, 2006.
- [17] X. Chen, Y. Wang, S. Gao, T.-P. Jung, and X. Gao, "Filter bank canonical correlation analysis for implementing a high-speed SSVEP-based brain-computer interface," *Journal of Neural Engineering*, vol. 12, p. 046008, jun 2015.
- [18] R. Zerafa, T. Camilleri, O. Falzon, and K. Camilleri, "To train or not to train? a survey on training of feature extraction methods for ssvep-based bcis," *Journal of Neural Engineering*, vol. 15, 06 2018.
- [19] H. Hotelling, "Relations between two sets of variates," *Biometrika*, vol. 28, no. 3/4, pp. 321–377, 1936.
- [20] K. F. Lao, C. M. Wong, Z. Wang, and F. Wan, "Learning prototype spatial filters for subject-independent ssvep-based brain-computer interface," in *IEEE International Conference on Systems, Man, and Cybernetics (SMC)*, pp. 485–490, 2018.
- [21] C. M. Wong, F. Wan, B. Wang, Z. Wang, W. Nan, K. F. Lao, P. U. Mak, M. I. Vai, and A. Rosa, "Learning across multi-stimulus enhances target recognition methods in SSVEP-based BCIs," *Journal of Neural Engineering*, vol. 17, no. 1, p. 016026, 2020.
- [22] O. Berke Güney, D. Küçükahmetler, R. Çiftçiöğlu, G. Coşkun, and H. Özkan, "Unsupervised adaptation of dnn for brain-computer interface spellers," in *2022 30th Signal Processing and Communications Applications Conference (SIU)*, pp. 1–4, 2022.
- [23] J. Liang, D. Hu, and J. Feng, "Do we really need to access the source data? source hypothesis transfer for unsupervised domain adaptation," in *Proceedings of the 37th International Conference on Machine Learning, ICML'20*, 2020.
- [24] S. Yang, Y. Wang, J. van de weijer, L. Herranz, and S. JUI, "Exploiting the intrinsic neighborhood structure for source-free domain adaptation," in *Advances in Neural Information Processing Systems*, 2021.
- [25] L. Yi, G. Xu, P. Xu, J. Li, R. Pu, C. Ling, I. McLeod, and B. Wang, "When source-free domain adaptation meets learning with noisy labels," in *The Eleventh International Conference on Learning Representations (ICLR)*, 2023.
- [26] I. Martišius and R. Damaševičius, "A prototype ssvep based real time bci gaming system," *Computational intelligence and neuroscience*, 2016.
- [27] J. R. Wolpaw, N. Birbaumer, D. J. McFarland, G. Pfurtscheller, and T. M. Vaughan, "Brain-computer interfaces for communication and control," *Clinical Neurophysiology*, vol. 113, no. 6, pp. 767–791, 2002.

- [28] A. P. Dempster, N. M. Laird, and D. B. Rubin, “Maximum likelihood from incomplete data via the em algorithm,” *Journal of the Royal Statistical Society. Series B (Methodological)*, vol. 39, no. 1, pp. 1–38, 1977.
- [29] J. Liang, D. Hu, and J. Feng, “Domain adaptation with auxiliary target domain-oriented classifier,” in *2021 IEEE/CVF Conference on Computer Vision and Pattern Recognition (CVPR)*, pp. 16627–16637, 2021.
- [30] D.-H. Lee, “Pseudo-label: The simple and efficient semi-supervised learning method for deep neural networks,” in *Workshop on challenges in representation learning, ICML*, vol. 3, 2013.
- [31] Y. Grandvalet and Y. Bengio, “Semi-supervised learning by entropy minimization,” in *Advances in Neural Information Processing Systems*, vol. 17, MIT Press, 2004.
- [32] K. Nigam, A. K. McCallum, S. Thrun, and T. Mitchell, “Text classification from labeled and unlabeled documents using em,” *Machine learning*, vol. 39, no. 2, pp. 103–134, 2000.
- [33] N. Srivastava, G. Hinton, A. Krizhevsky, I. Sutskever, and R. Salakhutdinov, “Dropout: A simple way to prevent neural networks from overfitting,” *Journal of Machine Learning Research*, vol. 15, no. 56, pp. 1929–1958, 2014.
- [34] B. Kulis, “Metric learning: A survey,” *Foundations and trends in machine learning*, vol. 5, no. 4, pp. 287–364, 2012.
- [35] A. K. Massimino and M. A. Davenport, “As you like it: Localization via paired comparisons,” *arXiv*, 2018.
- [36] M. Gönen and E. Alpaydin, “Multiple kernel learning algorithms,” *The Journal of Machine Learning Research*, vol. 12, pp. 2211–2268, 2011.
- [37] P. J. Rousseeuw, “Silhouettes: A graphical aid to the interpretation and validation of cluster analysis,” *Journal of Computational and Applied Mathematics*, vol. 20, pp. 53–65, 1987.
- [38] Y. Zou, Z. Yu, X. Liu, B. Kumar, and J. Wang, “Confidence regularized self-training,” in *2019 IEEE/CVF International Conference on Computer Vision (ICCV)*, (Los Alamitos, CA, USA), pp. 5981–5990, IEEE Computer Society, nov 2019.

VII. APPENDIX: IMPLEMENTATION DETAILS

In this section, we explain the implementation details of the utilized DNN architecture [3], the neighbor selection as well as confidence of the instances. Our code is available at <https://github.com/osmanberke/SFDA-SSVEP-BCI>

A. The DNN Architecture

The utilized DNN [3] consists of four convolutional and one fully connected layers. The first convolutional layer combines the sub-bands, whereas the second combines the channels. The third and fourth convolutional layers extract the features by processing the EEG signals in time and the last fully connected layer obtains the spelled character prediction. This DNN architecture achieves the best reported accuracy and ITR results on the benchmark [11] and BETA [12] datasets to date, when it is trained in a supervised setting.

We refer the interested reader to [3] for the full description.

B. Neighbor Selection

As the EEG instances \mathbf{x}_i ’s are multidimensional, the correlation coefficient between two given instances cannot be calculated regularly by $\rho(\mathbf{a}, \mathbf{b}) = \frac{\mathbf{a}\mathbf{b}'}{\|\mathbf{a}\| \|\mathbf{b}\|}$ (assuming that the signals are zero mean row vectors, and \mathbf{b}' is the transpose of \mathbf{b}). We calculate this correlation coefficient after reducing the dimension by combining the channels of the instances with the channel combination weight $\mathbf{w}_c^{(*)}(\lambda) \in \mathbb{R}^{C \times 1}$ as follows:

$$\rho(\mathbf{w}_c^{(*)'}(\lambda)\mathbf{x}_i, \mathbf{w}_c^{(*)'}(\lambda)\mathbf{x}_j), \quad (5)$$

where $\mathbf{w}_c^{(*)'}(\lambda)$ is the transpose of $\mathbf{w}_c^{(*)}(\lambda)$ and λ is the weighting of the two terms in the final loss. Hence, all the

equations in main text containing the correlation coefficient are dependent on the channel combination weights $\mathbf{w}_c^{(*)}(\lambda)$, including the distance term $d(\mathbf{x}_j, \mathbf{x}_i)$ in (4). Note also that, with a slight abuse of notation, the correlation coefficient notation $\rho(\mathbf{x}_i, \mathbf{x}_j)$ in main text in fact refers to the computation after combining the channels as in (5). Consequently, the silhouette score of the instance $m_i(\lambda)$ and the overall silhouette score $m(\lambda)$ become dependent of $\mathbf{w}_c^{(*)}(\lambda)$, which we denote in this section by $m_i(\lambda, \mathbf{w}_c^{(*)}(\lambda))$, $m(\lambda, \mathbf{w}_c^{(*)}(\lambda))$, respectively, but do not show it in the main text for simplicity in exposition.

On the other hand, the channel combination $\mathbf{w}_c^{(*)}(\lambda)$ is selected to maximize the overall silhouette score for the given predictions. The reason behind this selection is that the channel combination that maximizes the metric performance (i.e. silhouette score) is intuitively expected to describe the user’s spatial characteristics well. However, since the direct maximization of this score is intractable, we follow a different strategy, and select the channel combination $\mathbf{w}_c^{(*)}(\lambda)$ that maximizes the overall silhouette score $m(\lambda, \mathbf{w}_c^{(*)}(\lambda))$ among the finite set of channel combination weights from the second layer (i.e. channel combination layer) of the DNN as

$$\mathbf{w}_c^{(*)}(\lambda) = \arg \max_{\mathbf{w}_c(\lambda) \in \{\mathbf{w}_c(\lambda)\}_j} \frac{1}{N} \sum_{i=1}^N m_i(\lambda, \mathbf{w}_c(\lambda)).$$

Here, we stress that the variables actually change across (and so are further dependent on) iterations in our Algorithm 1. This, to be more precise, requires a superscript (t) in notation but we dropped it for simplicity here and in main text as well.

On the other hand, the weights in the channel combination layer are learned/tuned for the input whose sub-bands of harmonics (generated in the preprocessing step) are combined in the preceding DNN layer. Therefore, to effectively use the selected channel combination weights and to take advantage of the preprocessing step in the neighbors and silhouette score calculation, we first preprocess the original EEG input to generate the sub-bands of harmonics. Then, we combine the sub-bands with the weights from the sub-band combination layer, and then produce \mathbf{x}_i that is used in the calculation of the silhouette score as well as in the determination of the instances’ neighbors. Note also that the network weights are updated over iterations, so the channel and sub-band combination weights are also updated, which affect the calculation of the neighbors of instances. Hence, at each iteration t , the neighbors of instances must be recalculated: firstly, the channel combination is selected to maximize the silhouette score $m^{(t)}(\lambda, \mathbf{w}_c^{(t*)}(\lambda))$ for the given predictions, then, the neighbors of instances are determined with the selected channel combination.

C. Instance Confidence

In the loss term, we use the pseudo-labels of the instances having the positive silhouette score as explained in main text. However, with this strategy, there is a probability that either the self-adaptation term or the local-regularity term cease to be applicable for an instance \mathbf{x}_i at any iteration t . If the instance

itself has the negative silhouette score (i.e., $m_i^{(t)}(\lambda, \mathbf{w}_c^{(*)}) < 0$), the self-adaptation term becomes inapplicable; and if all the determined instance's neighbors have the negative silhouette score (i.e., $m_j^{(t)}(\lambda, \mathbf{w}_c^{(*)}) < 0, \forall j \in I_i^{(t)}$), the local-regularity term becomes inapplicable. Therefore, to enable the instances to contribute equally to the loss term; if one of the terms becomes inapplicable for the instance x_i , we update the λ term for that instance as follows:

$$\begin{aligned} \mathcal{L}_{total}^{(t)} = & \frac{-1}{N} \sum_{i=1}^N \lambda_i^{(t)} \log(\mathbf{s}_{i, \hat{y}_i^{(t)}}^{(t)}) \\ & + \frac{-1}{N} \sum_{i=1}^N \left[\frac{1 - \lambda_i^{(t)}}{k_i} \sum_{j=1}^{k_i} \log(\mathbf{s}_{i, \hat{y}_{I_i^{(t)}(j)}}^{(t)}) \right], \end{aligned}$$

where $\lambda_i^{(t)}$ is the instance specific λ term at iteration t and it equals to the global λ , if the both loss terms (self-adaptation and local-regularity) are applicable; and it equals to 0 or 1, if one of the term is inapplicable:

$$\lambda_i^{(t)} = \begin{cases} 1 & \text{if } m_j^{(t)}(\lambda, \mathbf{w}_c^{(*)}) < 0, \forall j \in I_i^{(t)} \\ 0 & \text{if } m_i^{(t)}(\lambda, \mathbf{w}_c^{(*)}) < 0 \\ \lambda & \text{otherwise} \end{cases}.$$

Even both terms may become inapplicable for some instances, then we do not use those instances in the loss.

D. Initial Predictions

The performance of the initial DNN model, which is pre-trained with data from source domains, may not be satisfactory for some target domains, especially when a majority of source domains' data statistics are much different from those of the target domain. In such cases, the completely training-free algorithms, such as FBCCA, might give better (more accurate) initial predictions. For this reason, we get initial predictions from either the pre-trained initial model or the FBCCA method. We choose the one having an initial higher silhouette score.